Earth and Planetary Science Letters ••• (••••) •••–•••

Contents lists available at ScienceDirect

Earth and Planetary Science Letters

www.elsevier.com/locate/epsl

# A complex history of silicate differentiation of Mars from Nd and Hf isotopes in crustal breccia NWA 7034

Rosalind M.G. Armytage [a,*], Vinciane Debaille [a], Alan D. Brandon [b], Carl B. Agee [c]

[a] Laboratoire G-Time, CP 160/02, Université Libre de Bruxelles, Av. F. Roosevelt 50, 1050 Bruxelles, Belgium
[b] Department of Earth and Atmospheric Sciences, University of Houston, Houston, TX, 77204, USA
[c] Institute of Meteoritics, University of New Mexico, Albuquerque, NM, 87131, USA

ARTICLE INFO

*Article history:*
Received 9 February 2018
Received in revised form 20 June 2018
Accepted 6 August 2018
Available online xxxx
Editor: W.B. McKinnon

*Keywords:*
Mars
silicate differentiation
shergottites
Hf isotopes
Nd isotopes

ABSTRACT

Resolving the possible mantle and crustal sources for shergottite meteorites is crucial for understanding the formation and early differentiation of Mars. Orbiter and rover characterization of the martian surface reveal that the major element composition of most of its surface does not match the shergottites (McSween et al., 2009) leaving the relationship between them poorly understood. The identification of the meteorite NWA 7034 and its pairs as a Mars surface rock (Cartwright et al., 2014) provides access to a representative sample of Mars' crust (Agee et al., 2013; Humayun et al., 2013). Utilizing the short-lived $^{146}Sm$–$^{142}Nd$, and long-lived $^{147}Sm$–$^{143}Nd$ and $^{176}Lu$–$^{176}Hf$ chronometers, which are sensitive to silicate differentiation, we analyzed three fragments of NWA 7034. The very negative mean isotopic compositions for this breccia, $\mu^{142}Nd_{JNdi\text{-}1} = -45 \pm 5$ (2SD), $\varepsilon^{143}Nd_{CHUR} = -16.7 \pm 0.4$ (2SD) and $\varepsilon^{176}Hf_{CHUR} = -61 \pm 9$ (2SD) point to an ancient origin for this martian crust. However, modeling of the data shows that the crust sampled by NWA 7034 possesses a Hf/Nd ratio and coupled $\varepsilon^{143}Nd$–$\mu^{142}Nd$ model age that are incompatible with this crustal reservoir being an end-member that generated the shergottite source mixing array. In addition, this crust is not juvenile, despite its rare earth element profile, but has had a multistage formation history. Therefore, early crustal extraction alone was not responsible for the creation of the reservoirs that produced the shergottites. Instead mantle reservoirs formed via other early differentiation processes such as in a Mars magma ocean must be responsible for the trace element and isotopic signatures present in shergottites.



## 1. Introduction

The martian shergottite meteorites have a range of igneous crystallization ages from ~170 Myr to ~574 Myr (Nyquist et al., 2001; Brennecka et al., 2014). They exhibit significant variation in their incompatible trace element (ITE) contents and radiogenic isotopic compositions, indicative of multiple distinct sources (e.g. Borg et al., 2002). Based on these bulk rock characteristics, shergottites fall into three subgroups (depleted, intermediate, and enriched), forming compositional arrays that can be generated by mixing between a martian reservoir depleted in ITE, and one that is more ITE-enriched. These reservoirs have also been shown to differ in redox state, with a range in oxygen fugacity −2.5 to −1 log units relative to the quartz–fayalite–magnetite buffer (e.g. Herd et al., 2002). The depleted end-member is thought to represent the depleted martian mantle (Borg and Draper, 2003; Debaille et al., 2007, 2008). The enriched end-member reservoir remains enigmatic with both the martian crust (Humayun et al., 2013) or ITE-enriched late cumulates resulting from the crystallization of a martian magma ocean (Blichert-Toft et al., 1999; Borg and Draper, 2003; Debaille et al., 2007) being proposed. From coupling the short-lived $^{146}Sm$–$^{142}Nd$ and long-lived $^{147}Sm$–$^{143}Nd$ chronometers in shergottites, the resultant mixing line between their sources has been interpreted as a planetary isochron, representing either a single major differentiation event on Mars ~50 Myr after solar system formation (SSF) (Borg et al., 2003; Caro et al., 2008), or the termination of protracted crystallization of a martian magma ocean (MMO) ~100 Myr after SSF (Debaille et al., 2007, 2009). As such, identifying the enriched end-member for the shergottite mixing array is crucial for understanding the nature of differentiation on early Mars and its timing.

The martian crust is an obvious candidate for the enriched end-member reservoir that is added to shergottite magmas through assimilation-fractional crystallization (AFC) processes, as ITEs will be concentrated in the extracted melts that cool to form crust

* Corresponding author. Now at: Jacobs/JETS, NASA Johnson Space Center, 2101 NASA Parkway, Mailcode XI3, Houston, TX, 77058, USA.
*E-mail address:* rosalind.m.armytage@nasa.gov (R.M.G. Armytage).

https://doi.org/10.1016/j.epsl.2018.08.013
0012-821X/

during silicate differentiation. Explaining the shergottite ITE and isotopic compositional arrays in terms of crustal AFC is problematic when considered in conjunction with the textural diversity and major element variations in these meteorites (Borg and Draper, 2003; Ferdous et al., 2017). In addition, a crustal contamination origin does not easily replicate the correlation between the initial $\varepsilon^{143}$Nd and $\gamma^{187}$Os in shergottites (Brandon et al., 2012). An alternative scenario where the enriched mantle source formed as a late-stage residual melt during crystallization of a MMO (Borg et al., 2016; Brandon et al., 2012; Debaille et al., 2007) can account for the decoupling. The similarity of many of the compositional outcomes for shergottites in both scenarios, requires additional independent constraints to examine their relative likelihood, and hence our understanding of the early evolution of Mars.

The discovery of a unique martian polymict breccia meteorite (NWA 7034 meteorite, and its pairs, Agee et al., 2013; Humayun et al., 2013), and the confirmation of its martian origin (Cartwright et al., 2014) allows for such additional testing of the two scenarios. The major element composition of NWA 7034 matches the orbital and rover data bulk compositions of the martian crust (Agee et al., 2013; Humayun et al., 2013), unlike shergottites which do not match the composition of majority of the martian surface (McSween et al., 2009). The meteorite contains clasts with 4.428 Ga igneous zircons (Humayun et al., 2013) consistent with ancient exposed crust on Mars, and older than the 4.1 Ga orthopyroxenite ALH 84001 (Lapen et al., 2010). The clast types in NWA 7034 include igneous lithologies (basalt, basaltic andesite, trachyandesite, and a Fe–Ti–P rich lithology) as well as sedimentary, and those of impact origin (Santos et al., 2015). Despite the textural diversity and major element composition variation between the clasts, the trace element profiles of the component clasts as well as the matrix are remarkably similar, with the exception of the monzonite (similar to the trachyandesite from Santos et al., 2015) clasts (Humayun et al., 2013). The ITE concentrations in bulk analyses of NWA 7034 are considerably higher than in enriched shergottites, and their rare earth element (REE) patterns emulate a partial melt of a primitive mantle composition (Humayun et al., 2013), a signature of "juvenile" crust that conflicts with the petrologic diversity in the clasts (Hewins et al., 2016; Santos et al., 2015). As such this meteorite represents ancient crustal material that could conceivably be the enriched end-member reservoir for the shergottite source mixing arrays, providing a unique opportunity to test this hypothesis that has implications for the earliest differentiation history of Mars.

Radiogenic chronometers sensitive to silicate differentiation such as $^{146,147}$Sm–$^{142,143}$Nd and $^{176}$Lu–$^{176}$Hf can address whether crust represented by NWA 7034 is the ITE enriched end-member for shergottites, and also provide constraints on the formation of currently exposed ancient martian crust. Here we report $^{146,147}$Sm–$^{142,143}$Nd and $^{176}$Lu–$^{176}$Hf systematics, and REE abundances for three bulk breccia fragments of NWA 7034. Modeling of the chemical and isotopic data was carried out to determine the origin of the NWA 7034 crust and its relationship to the shergottites, and explore the concomitant implications for the early silicate differentiation history of Mars.

## 2. Methods

### 2.1. Sample preparation and chemistry

As NWA 7034 is a polymict breccia (e.g. Santos et al., 2015), three separate bulk fragments A, B, and C (fragments 1, 2, and 3 from Goderis et al., 2016) were measured to assess any possible isotopic heterogeneity. The three chips of NWA 7034 were individually crushed using an agate pestle and mortar, specific to achondrite samples. The respective dissolved sample powder masses were 123.4 mg, 118.2 mg, and 106.4 mg. Dissolution was initially by HF-$HNO_3$ in Savillex vials on the hotplate at 110 °C. An additional dissolution step was carried out in Parr bombs at 120 °C to ensure the destruction of refractory phases such as zircon. The resulting fluorides were attacked with multiple steps of HCl evaporation to ensure clear solutions. Subsequent to dissolution, a ∼5% aliquot was removed and spiked with a $^{176}$Lu–$^{179}$Hf and a $^{150}$Sm–$^{148}$Nd spike. These aliquots were passed over a four-column procedure to isolate Hf, Nd, Sm and Lu, beginning with a cation exchange resin to isolate a Hf cut and a REE (rare earth element) cut from the matrix. The REEs were subsequently separated from each other using HDEHP (di(2-ethylhexyl)orthophosphoric acid) resin, created in-house from Teflon beads and HDEHP. The Hf cut was purified using first an anion column to remove Fe, followed by an Ln-spec column (Eichrom). Two other ∼5% aliquots were removed, one for trace element analysis on the 7700 Agilent ICP-MS (inductively-coupled-plasma mass spectrometer) at Université Libre de Bruxelles (Table 1), and an additional 5% aliquot was removed for future possible isotope analysis. The remainder was passed over a seven column procedure to isolate Nd, Hf and Sm for isotopic ratio analysis. The main difference from the chemistry for the spiked aliquots (besides using a separate set of columns and smaller mesh sizes) is the purification of the REE cut. After the first pass on the HDEHP column, the Nd cut is oxidized with a $NaBrO_3$-10M $HNO_3$ mixture and passed over another, smaller HDEHP column to remove the oxidized Ce (modified after Li et al., 2015). The cut is then passed over a 0.5 ml cation resin column to remove the Na prior to analysis. The Sm cut is passed a second time over the HDEHP column, but with a slight change in acid molarity to ensure the complete removal of possible Nd interferences. Total procedural blanks are on the order of Hf < 160 pg, Lu < 26 pg, Nd < 74 pg and Sm < 6 pg, where the mass of each element that was processed was on the order Hf ∼ 500 ng, Lu ∼ 40 ng, Nd ∼ 1500 ng, and Sm ∼ 400 ng.

### 2.2. Isotope mass spectrometry

All the elemental and isotope analyses were carried out at Université Libre de Bruxelles (ULB). The spiked aliquots and the unspiked Hf were measured on the Nu Instruments Nu Plasma HR multi-collector inductively-coupled-plasma mass spectrometer (MC-ICP-MS) using an Aridus II desolvator. The unspiked Hf was introduced into the plasma using a 75 µl/min nebulizer and an Aridus II desolvator. The samples were bracketed every two samples using the JMC 475 standard to correct for mass fractionation. Potential isobaric interferences were monitored using $^{175}$Lu, $^{172}$Yb and $^{182}$W and found to be below the level of detection. The mean value for the standard was $^{176}$Hf/$^{177}$Hf = 0.282174 ± 0.00019 ($n = 20$) and the sample data were normalized to the literature value of $^{176}$Hf/$^{177}$Hf = 0.282163 ± 0.00009 (Blichert-Toft et al., 1997) (Table 2). The spiked aliquots were run at concentrations between 10–25 ppb, and corrected for mass fractionation using an exponential law followed by spike stripping using an iterative method (Debaille et al., 2007). The error on the $^{147}$Sm/$^{144}$Nd and $^{176}$Lu/$^{177}$Hf ratios is taken to be 5%, based on previous analysis of total procedural replicates, though the errors on the individual concentrations are much smaller as they are based purely on that of the spike, which is better than 0.5%. The measured $^{147}$Sm/$^{144}$Nd and $^{176}$Lu/$^{177}$Hf ratios of an aliquot of the USGS (US Geological Survey) standard BHVO-2, processed the same way, were 0.155, and 0.0093 respectively. These values correspond to the reference values of $^{147}$Sm/$^{144}$Nd = 0.150 and $^{176}$Lu/$^{177}$Hf = 0.0097 (Wilson, 1997), which are within the assigned 5% uncertainty. The unspiked high-precision Sm and Nd isotopic analyses were carried out on the Triton Plus TIMS (thermal ionization mass spectrometer) instrument also at ULB. Both were run on double Re filaments loaded

Please cite this article in press as: Armytage, R.M.G., et al. A complex history of silicate differentiation of Mars from Nd and Hf isotopes in crustal breccia NWA 7034. Earth Planet. Sci. Lett. (2018), https://doi.org/10.1016/j.epsl.2018.08.013

**Table 1**
Trace element concentrations in ppm.

| Element | NWA 7034-A | NWA 7034-B | NWA 7034-C | 2RSD (%)* | BHVO-2 (this study) | BHVO-2 (Wilson, 1997) | 2σ |
|---|---|---|---|---|---|---|---|
| Rb | 7.5 | 11.3 | 18.0 | 6.9 | 9.3 | 9.8 | 1 |
| Sr | 108.7 | 121.9 | 128.3 | 10.6 | 379 | 389 | 23 |
| Y | 27.1 | 22.8 | 24.3 | 9.2 | 26.8 | 26 | 2 |
| Zr | 159.5 | 112.9 | 115.8 | 1.4 | 163.1 | 172 | 11 |
| Nb | 13.9 | 11.0 | 11.0 | 2.4 | 17.2 | 18 | 2 |
| Ba | 73.4 | 79.5 | 91.9 | 16.9 | 143.9 | 130 | 13 |
| La | 10.7 | 8.3 | 8.8 | 2.2 | 16.6 | 15 | 1 |
| Ce | 25.3 | 19.6 | 20.4 | 2.0 | 38.5 | 38 | 2 |
| Pr | 3.5 | 2.7 | 2.8 | 0.4 | 5.3 | | |
| Nd | 16.1 | 12.7 | 12.9 | 0.2 | 24.1 | 25.0 | 1.8 |
| Sm | 4.5 | 3.5 | 3.6 | 2.7 | 6.1 | 6.2 | 0.4 |
| Eu | 1.15 | 1.09 | 1.11 | 1.0 | 2.09 | | |
| Gd | 5.6 | 4.5 | 4.6 | 1.5 | 7.0 | 6.3 | 0.2 |
| Tb | 0.9 | 0.7 | 0.7 | 1.3 | 1.0 | 0.9 | |
| Dy | 5.32 | 4.21 | 4.23 | 3.3 | 5.30 | | |
| Ho | 1.12 | 0.89 | 0.90 | 1.2 | 1.02 | 1.04 | 0.04 |
| Er | 2.98 | 2.38 | 2.39 | 4.0 | 2.52 | | |
| Tm | 0.43 | 0.35 | 0.35 | 4.6 | 0.34 | | |
| Yb | 2.44 | 2.05 | 2.08 | 3.4 | 2.0 | 2.0 | 0.2 |
| Lu | 0.36 | 0.32 | 0.31 | 8.7 | 0.29 | 0.28 | 0.01 |
| Hf | 4.00 | 2.70 | 2.69 | 4.2 | 3.99 | 4.1 | 0.3 |
| U | 0.41 | 0.30 | 0.30 | 5.0 | 0.39 | | |

All data reported in this table were collected by ICP-MS.
* 2RSD calculated from repeat analyses of BHVO-2 in the same measurement session.

**Table 2**
NWA 7034 isotopic data.

| | NWA 7034-A | ±2σ | NWA 7034-B | ±2σ | NWA 7034-C | ±2σ |
|---|---|---|---|---|---|---|
| Weight (g) | 0.1234 | | 0.1182 | | 0.1064 | |
| Sm (ppm)[a] | 4.5 | | 3.3 | | 3.3 | |
| Nd (ppm)[a] | 15.8 | | 11.8 | | 11.6 | |
| $(^{147}Sm/^{144}Nd)$[b] | 0.172 | 0.009 | 0.169 | 0.009 | 0.172 | 0.009 |
| $(^{143}Nd/^{144}Nd)_{meas}$[c] | 0.511765 | 0.000001 | 0.511779 | 0.000001 | 0.511781 | 0.000001 |
| $\varepsilon^{143}Nd_{CHUR}$ (present)[d] | −16.88 | 0.02 | −16.60 | 0.03 | −16.57 | 0.02 |
| $\mu^{142}Nd$[e] | −48 | 2 | −43 | 3 | −45 | 3 |
| $^{149}Sm/^{152}Sm$ | 0.516863 | 0.000002 | 0.516866 | 0.000002 | 0.516862 | 0.000004 |
| $^{150}Sm/^{152}Sm$ | 0.276002 | 0.000001 | 0.276017 | 0.000001 | 0.276022 | 0.000005 |
| Lu (ppm)[a] | 0.41 | | 0.32 | | 0.30 | |
| Hf (ppm)[a] | 4.84 | | 3.11 | | 3.08 | |
| $(^{176}Lu/^{177}Hf)_{meas}$ | 0.0121 | 0.006 | 0.0145 | 0.007 | 0.0140 | 0.007 |
| $(^{176}Hf/^{177}Hf)_{meas.}$[f] | 0.280903 | 0.000019 | 0.281124 | 0.000019 | 0.281123 | 0.000019 |
| $\varepsilon^{176}Hf_{CHUR}$ (present)[g] | −66.5 | 0.7 | −58.7 | 0.7 | −58.8 | 0.7 |

[a] Concentrations from spiked aliquots.
[b] Measured ratio with uncertainty of 5% (see text for details).
[c] Ratio has been corrected to published value for JNdi-1 from Tanaka et al. (2000), and the reported uncertainties are 2 standard error of the mean.
[d] $\varepsilon^{143}Nd_{CHUR}$ (present) is $([(^{143}Nd/^{144}Nd)_{meas.}/(^{143}Nd/^{144}Nd)_{CHUR}]-1))\times 10^4$. and where $(^{143}Nd/^{144}Nd)_{CHUR} = 0.512630$ (Bouvier et al., 2008).
[e] $\mu^{142}Nd$ is calculated by $([(^{142}Nd/^{144}Nd)_{meas.}/(^{142}Nd/^{144}Nd_{standard}]-1))\times 10^6$, where $(^{142}Nd/^{144}Nd)_{standard}$ is the mean composition of JNdi-1in the turret which is 1.141835.
[f] The $(^{176}Hf/^{177}Hf)_{meas}$ ratio has been corrected to the published value of the JMC standard (Blichert-Toft et al., 1997) and the uncertainty is the 2 standard deviation of JMC 475 during the run.
[g] $\varepsilon^{176}Hf_{CHUR} = [((^{176}Hf/^{177}Hf)_{meas.}/(^{176}Hf/^{177}Hf)_{CHUR}) - 1]\times 10^4$, where $(^{176}Hf/^{177}Hf)_{CHUR} = 0.282785$ (Bouvier et al., 2008).

in 5 µl 0.7 M $H_3PO_4$ and measured as positive metal ions. The measured Nd data are normalized to $^{146}Nd/^{144}Nd = 0.7219$ to correct for instrumental mass fractionation during the runs (Supplementary Table 1). Potential $^{142}Ce$ and $^{144,148,150}Sm$ interferences were monitored using $^{140}Ce$ and $^{147}Sm$. Corrections for the Ce interference were <2.5 ppm and Sm was within the noise on the Faraday collector. The Nd was run using a three line multi-static routine (Caro et al., 2006; Debaille et al., 2007) where the amplifiers are rotated between blocks. The JNdi-1 standards run in the same turret had a mean $^{142}Nd/^{144}Nd$ value of 1.141836 ± 0.000003 (2SD, $n = 4$) and $^{143}Nd/^{144}Nd = 0.512099 \pm 0.000001$ (2SD, $n = 4$), which is consistent with the long-term standard average for this instrument of $^{142}Nd/^{144}Nd = 1.141836 \pm 0.000005$ (2SD, $n = 28$) and $^{143}Nd/^{144}Nd = 0.512099 \pm 0.000001$ (2SD, $n = 28$) without changing the position of the cups. The turret average is used as the normalizing value for $\mu^{142}Nd$. The high precision Sm isotopic compositions were normalized to $^{147}Sm/^{152}Sm = 0.569828$ to correct for instrumental mass fractionation using the exponential law (Supplementary Table 2). The AMES standards run in the same turret had a mean $^{149}Sm/^{152}Sm$ of 0.516887 ± 0.000003 (2SD, $n = 4$) and $^{150}Sm/^{152}Sm = 0.276002 \pm 0.000002$ (2SD, $n = 4$), consistent with the long term averages for this instrument of $^{149}Sm/^{152}Sm = 0.516887 \pm 0.000005$ (2SD, $n = 30$), and $^{150}Sm/^{152}Sm = 0.276003 \pm 0.000003$ (2SD, $n = 30$).

To check the accuracy of the isotopic measurements, an aliquot of the USGS standard BHVO-2 was passed through the identical chemical procedure as the NWA 7034 fragments. The Hf and Nd isotopic compositions BHVO-2 were $^{176}Hf/^{177}Hf = 0.283109 \pm 0.000019$ (2SD) and $^{143}Nd/^{144}Nd = 0.512986 \pm 0.000001$ (2SE). These values are in excellent agreement with the reported liter-

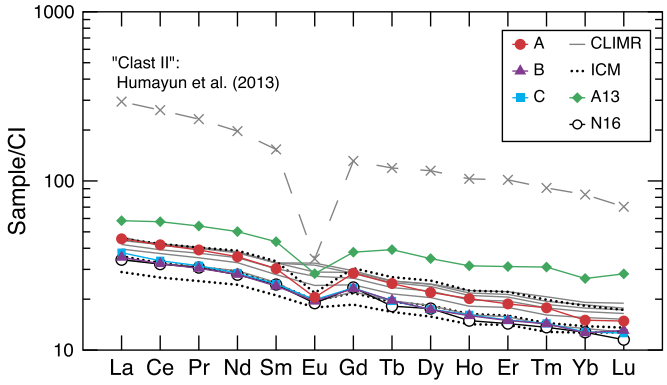


**Fig. 1.** Rare earth element profiles from samples of NWA 7034 and its pairings normalized to CI abundances (Anders and Grevesse, 1989). A, B and C refer to the three different aliquots of NWA 7034 analyzed in this study. ICM and CLIMR refer to interclast crystalline matrix and clast laden impact melt rock respectively and are selected analyses thought to be representative of the average REE composition for the NWA 7034 breccia (Humayun et al., 2013). Also plotted are previous whole rock analyses for NWA 7034: A13 and N16 from Agee et al. (2013) and Nyquist et al. (2016) respectively. The whole rock composition from Agee et al. (2013) appears to be leveraged by a more "exotic" clast such as Clast II (Humayun et al., 2013).

ature values for BHVO-2 of $^{176}Hf/^{177}Hf = 0.283105 \pm 0.000011$ (2SD) (Weis et al., 2007) and $^{143}Nd/^{144}Nd = 0.512984 \pm 0.000011$ (2SD) (Weis et al., 2006).

## 3. Results

### 3.1. Trace element concentrations

The trace element concentrations measured by ICP-MS for NWA 7034 fragments A, B, and C are presented in Table 1. The rare earth element (REE) compositions of the three fragments of NWA 7034 fall in the range defined by the majority of the clasts and matrix (Humayun et al., 2013), indicating that the $^{143}Nd/^{144}Nd$, $^{142}Nd/^{144}Nd$, and $^{176}Hf/^{177}Hf$, likely reflect the "bulk" breccia composition rather than being leveraged by the more "exotic" family of clasts (trachyandesite, norite) identified in previous studies (Humayun et al., 2013; Santos et al., 2015) (Fig. 1). The REE concentrations of fragment A are ~25% higher than fragments B and C, but still fall within the compositional range defined by analyses of interclast crystalline matrix (ICM) and clast laden impact melt rock (CLIMR) by Humayun et al. (2013).

### 3.2. Isotopic data

In Table 2 (and hereon) the measured $^{143}Nd/^{144}Nd$ and $^{176}Hf/^{177}Hf$ isotope ratios are presented in $\varepsilon$ notation (deviation in parts per $10^4$ from the chondritic uniform reservoir (CHUR): $^{143}Nd/^{144}Nd = 0.512630 \pm 11$; $^{176}Hf/^{177}Hf = 0.282785 \pm 11$; Bouvier et al., 2008) and the $^{142}Nd/^{144}Nd$ ratios are presented using $\mu$ notation (deviation in parts per $10^6$ from the JNdi-1 terrestrial standard). The three fragments of NWA 7034 have indistinguishable $\varepsilon^{143}Nd$ and $\mu^{142}Nd$ within error, with an average $\varepsilon^{143}Nd$ of $-16.7 \pm 0.4$ (2SD) and $\mu^{142}Nd$ of $-45 \pm 5$ (2SD). The $^{148}Nd/^{144}Nd$ and $^{150}Nd/^{144}Nd$ ratios show no deviation from terrestrial within analytical precision (Supplementary Table 1), consistent with the recent data for martian meteorites in Kruijer et al. (2017). The $\varepsilon^{176}Hf$ isotopic compositions show variation outside of external reproducibility with fragment A having a composition of $-66.5 \pm 0.7$ (2SD), while B and C are within uncertainty of each other, $\varepsilon^{176}Hf = -58.7 \pm 0.7$ (2SD), and $\varepsilon^{176}Hf = -58.8 \pm 0.7$ (2SD) giving a mean value for NWA 7034 of $\varepsilon^{176}Hf = -61 \pm 9$ (2SD).

As NWA 7034 is an ancient surface breccia (e.g. McCubbin et al., 2016), it may have experienced exposure to galactic cosmic rays and there may also be contributions from chondritic impactors. Both of these effects need to be accounted for prior to using the measured isotopic data to put constraints on the silicate differentiation history of Mars. The reaction $^{149}Sm(n, \gamma)^{150}Sm$ can be used as a dosimeter as $^{149}Sm$ has a thermal neutron cross section that is orders of magnitude greater than $^{142,144}Nd$ or $^{176,177}Hf$ (Nyquist et al., 1995; Sprung et al., 2013). A linear correlation between $^{150}Sm/^{152}Sm$ versus $^{149}Sm/^{152}Sm$ with a slope of $-1$ should be observed if these fragments had experienced significant neutron fluence. However, Supplementary Fig. 1 shows that such a relationship does not exist, and the data from NWA 7034 overlap with terrestrial basalts. Therefore, as with the much younger shergottites (Borg et al., 2016), no correction of the measured $^{142}Nd/^{144}Nd$, $^{143}Nd/^{144}Nd$, or $^{176}Hf/^{177}Hf$ isotopic ratios is required. Previous work on these three NWA 7034 fragments using highly siderophile elements and Os isotopes puts the contribution of chondritic impactor at ~3 wt% (Goderis et al., 2016). Based on mass balance calculations, the effect of this impactor addition for Sm, Nd, Lu, and Hf falls within analytical error, therefore the radiogenic isotope compositions reported here reflect interior martian processes, rather than chondritic contamination. The measured variation in $^{176}Hf/^{177}Hf$ between fragment A versus B and C is therefore attributed to an effect of the polymict brecciated nature of NWA 7034, and the fact that Lu and Hf have very different mineralogical affinities from one another.

## 4. Discussion

### 4.1. Relationship between NWA 7034 and shergottites

The very negative $\varepsilon^{143}Nd$ and $\varepsilon^{176}Hf$ values correspond to an enriched early differentiated crustal signal, consistent with the U–Pb ages of zircons, baddeleyites, and feldspars in the NWA 7034 meteorite (Bellucci et al., 2015; Humayun et al., 2013), as well the Sm–Nd age of 4.44 Ga of the bulk matrix domain (Nyquist et al., 2016). The negative isotopic values, coupled with the trace element data, suggest at the "bulk" breccia level, the isotopic analyses performed in this study likely reflect an ancient enriched reservoir, and the associated differentiation processes, rather than more recent (<4.4 Ga) crustal evolution.

As previously observed, the $\varepsilon^{143}Nd$ versus La/Yb for NWA 7034 plots as an enriched end-member on a two-component mixing hyperbola for shergottites (Agee et al., 2013), with the least-squares regression (LSR) curve being reproduced by mixing between NWA 7034 and the depleted shergottite QUE 94201 (Fig. 2a). However, this corroboration of the crust contamination hypothesis is not strongly supported by our new $\varepsilon^{176}Hf$ data (Fig. 2b), because the purely mathematical LSR curve cannot be satisfactorily reconstructed with QUE 94201, Tissint, or the older ~2.4 Ga martian basalt NWA 7635 (Lapen et al., 2017) as the depleted end-member if NWA 7034 is taken as the enriched reservoir.

A more accurate evaluation of the possible existence of mixing relationships is to plot the calculated source compositions, which allows for the contemporaneous comparison of end-members, as the radiogenic ingrowth for the range of shergottite crystallization ages must be considered. Table 3 contains the calculated source compositions for the individual martian meteorites plotted in Figs. 3 & 4. Details of the calculations and the measured ratios can be found in the Supplementary Information, and Supplementary Table 3. Two proposed depleted reservoir compositions are plotted in Fig. 3, DMM (depleted martian mantle, Borg and Draper, 2003), and DSS (depleted shergottite source, Debaille et al., 2008). As in Fig. 2, crustal composition represented by NWA 7034 falls at the enriched end of the shergottite source array in $(Lu/Hf)_{source}$ vs $(Sm/Nd)_{source}$ space along a hyperbolic LSR (Fig. 3). Here the assumption is being made that the NWA 7034 crust represents

Please cite this article in press as: Armytage, R.M.G., et al. A complex history of silicate differentiation of Mars from Nd and Hf isotopes in crustal breccia NWA 7034. Earth Planet. Sci. Lett. (2018), https://doi.org/10.1016/j.epsl.2018.08.013

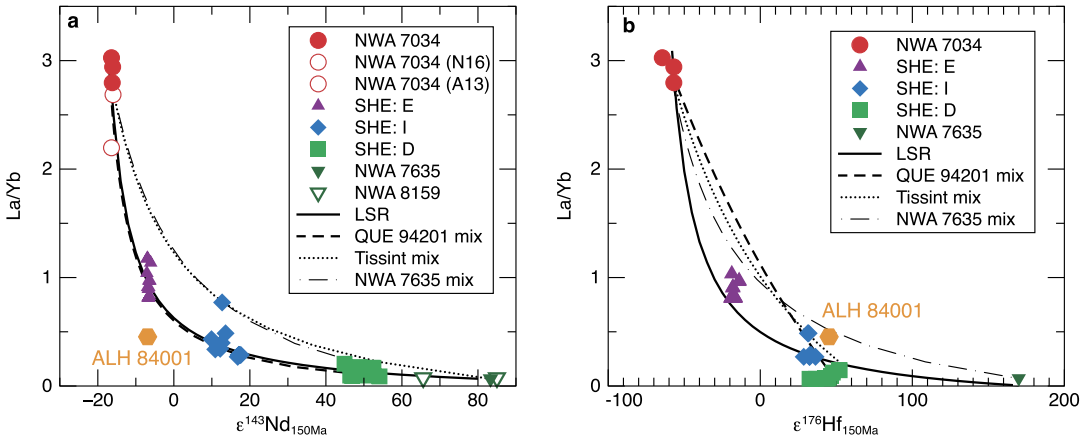


**Fig. 2.** Bulk rock chondritic normalized La/Yb plotted against (a) $\varepsilon^{143}$Nd and (b) $\varepsilon^{176}$Hf calculated at 150 Ma for NWA 7034 (this study; A13: Agee et al., 2013; N16: Nyquist et al., 2016), shergottites (Blichert-Toft et al., 1999; Borg et al., 2016; Debaille et al., 2007), NWA 7635 (Lapen et al., 2017), NWA 8159 (Herd et al., 2017) and ALH 84001 (Lapen et al., 2010) (see Table 3 for literature values). The La/Yb ratios are from numerous sources shown in Supplementary Table 3. ALH 84001 is included for comparison purposes, and is not included in any of the regressions or calculations. Only literature data where both parent–daughter ratios and isotopic measurements have been published for the same dissolution have been included (see Supplementary Table 3 for details of literature data). The bulk rock La/Yb ratios in most cases are unfortunately not from the same dissolution. The LSR curve is a least squares regression through all the data excluding ALH 84001. The mixing curves are simple binary mixing curves, using an average of the three NWA 7034 fragments from this study as one end member, and other end member stated in the legend.

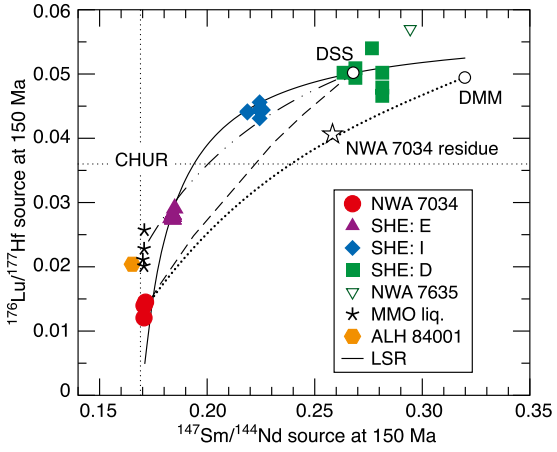


**Fig. 3.** Source $^{176}Lu/^{176}Hf$ versus $^{147}Sm/^{144}Nd$ calculated at 150 Ma. See Supplementary Information for details of the source calculations. The LSR is a least squares regression fit through all the plotted meteorite data (with the exception of ALH 84001, Lapen et al., 2010). DMM is a depleted martian mantle composition ($^{147}Sm/^{144}Nd = 0.303$; $^{176}Lu/^{177}Hf = 0.0504$; Borg and Draper, 2003), DSS is a depleted shergottite source composition ($^{147}Sm/^{144}Nd = 0.2679$; $^{176}Lu/^{177}Hf = 0.0502$; Debaille et al., 2008), with the MMO liquid compositions coming from the same study. The NWA 7034 residue composition is calculated based on the extraction of a 4% melt of a primitive mantle composition (McDonough and Sun, 1995), using a martian mantle mineralogy (Borg and Draper, 2003). The dashed and dotted lines represent binary mixing models between NWA 7034 and DSS or DMM respectively. The dotted–dashed line is a calculated mix between the liquids after 98% fractional crystallization of a 1350 km deep magma ocean ($^{147}Sm/^{144}Nd = 0.1701$; $^{176}Lu/^{177}Hf = 0.0211$) and DSS (Debaille et al., 2008).

an end-member reservoir, and hence the actual rock composition rather than the source has been plotted. However, when using the actual Nd and Hf elemental and isotopic compositions, it is not possible to calculate a viable binary mixing curve through the shergottite data between NWA 7034 as the enriched end-member with any of the depleted shergottite source compositions (Fig. 3). Instead, an enriched composition similar to the one modeled for late stage liquids of a martian magma ocean (MMO) 1350 km deep (Debaille et al., 2008) is required to reproduce the mixing array of the shergottite sources (dash-dotted line, Fig. 3). Therefore, despite NWA 7034 being a sample of an ancient enriched martian reservoir, there must have been an additional large scale silicate differentiation process, to generate the enriched end-member of the shergottite source array. This is consistent with the preservation of multiple mantle reservoirs with different segregation histories via solidification of an MMO to generate the enriched and depleted source compositions expressed in shergottites (Debaille et al., 2008). One aspect of note in Fig. 3, is that the source composition of the other ancient martian meteorite, the orthopyroxenite ALH 84001, coincides with the required composition for the shergottite enriched reservoir, suggestive of a genetic link to the shergottites sources (Lapen et al., 2010, 2017).

There is a caveat, however to this conclusion from the coupled $^{147}Sm/^{144}Nd$–$^{176}Lu/^{177}Hf$ source modeling. Because the curve of the hyperbola is related to Hf/Nd ratios of the end-members (Langmuir et al., 1978), and as there is ample evidence that NWA 7034 is not a "pure" igneous crustal rock, but instead a polymict breccia (Humayun et al., 2013; Santos et al., 2015), it is possible that the measured Hf/Nd ratio of NWA 7034 in this study does not accurately reflect the Hf/Nd ratio of the enriched crustal reservoir that it is sampling, but may be perturbed by smaller scale mineralogical heterogeneities.

One way to examine the possibility of decoupling between the $^{147}Sm$–$^{143}Nd$ and $^{176}Lu$–$^{176}Hf$ chronometers due to the different mineralogical affinities of Hf and Nd, is to use the short-lived and long-lived radiogenic chronometers of $^{146}Sm$–$^{142}Nd$ ($t_{1/2}$ ~103 Myr) (Meissner et al., 1987) and $^{147}Sm$–$^{143}Nd$ ($t_{1/2}$ ~106 Gyr) to constrain the relationship between the crust represented by NWA 7034 and the shergottite array. These two coupled systems evolve with identical time-integrated Sm/Nd, allowing for calculation of two-stage source evolution models for NWA 7034 and shergottite sources. An additional advantage of coupling the two Sm–Nd chronometers is the possibility of extracting timing constraints for silicate differentiation. The two-stage model assumes radiogenic growth in an undifferentiated reservoir followed by silicate differentiation that results in Sm/Nd fractionation (Debaille et al., 2007; Rankenburg et al., 2006) (see supplementary information for details of the calculations). Mixing trends between end-members are straight lines and if the mixing line intersects the bulk planet initial $\varepsilon^{143}Nd$–$\mu^{142}Nd$ it can also represent an isochron, making the initial Nd isotopic composition a key variable in any model of martian silicate differentiation. Three scenarios have been explored to test possible relationships between NWA 7034 and the shergottites (Fig. 4).

Please cite this article in press as: Armytage, R.M.G., et al. A complex history of silicate differentiation of Mars from Nd and Hf isotopes in crustal breccia NWA 7034. Earth Planet. Sci. Lett. (2018), https://doi.org/10.1016/j.epsl.2018.08.013

**Table 3**
Calculated isotopic ratios and source composition.

| | $\varepsilon^{143}$Nd at 150 Ma[a] | $^{147}Sm/^{144}Nd$ source at 150 Ma[b] | $\varepsilon^{143}$Nd source at 150 Ma[d] | Reference | $\varepsilon^{176}$Hf at 150 Ma | $^{176}Lu/^{177}Hf$ source at 150 Ma | $\varepsilon^{176}$Hf source at 150 Ma | Reference |
|---|---|---|---|---|---|---|---|---|
| Breccia | | | | | | | | |
| NWA 7034-A | −16.4 | 0.1722[c] | −63.8 | This study | −64.4 | 0.0121[c] | −64.4 | This study |
| NWA 7034-B | −16.1 | 0.1691[c] | −67.0 | This study | −56.9 | 0.0145[c] | −56.9 | This study |
| NWA 7034-C | −16.1 | 0.1720[c] | −55.5 | This study | −56.9 | 0.0140[3] | −56.9 | This study |
| NWA 7034 | −16.0 | 0.1671[c] | −3.4 | Agee et al. (2013) | | | | |
| NWA 7034 | −16.4 | 0.1664[c] | −0.9 | Nyquist et al. (2016) | | | | |
| Enriched shergottites | | | | | | | | |
| Shergotty | −6.7 | 0.184 | −6.8 | Debaille et al. (2007) | −16.9 | 0.0281 | −16.9 | Debaille et al. (2008) |
| | | | | | −18.8 | 0.0274 | −18.7 | Blichert-Toft et al. (1999) |
| | | | | | −16.5 | 0.0282 | −16.4 | Blichert-Toft et al. (1999) |
| Zagami | −6.7 | 0.1840 | −6.9 | Debaille et al. (2007) | −16.6 | 0.0282 | −16.4 | Debaille et al. (2008) |
| | | | | | −19.1 | 0.0274 | −19.0 | Blichert-Toft et al. (1999) |
| | | | | | −17.6 | 0.0278 | −17.5 | Blichert-Toft et al. (1999) |
| NWA 856 | −6.6 | 0.1842 | −6.7 | Debaille et al. (2007) | −18.0 | 0.0278 | −17.7 | Debaille et al. (2008) |
| | −6.9 | 0.1836 | −7.1 | Borg et al. (2016) | | | | |
| Los Angeles | −6.3 | 0.1849 | −6.8 | Debaille et al. (2007) | −13.9 | 0.0291 | −13.7 | Debaille et al. (2008) |
| | −6.6 | 0.1841 | −6.8 | Borg et al. (2016) | | | | |
| Dhofar 378 | −6.7 | 0.1843 | −6.7 | Borg et al. (2016) | | | | |
| NWA 4878 | −6.7 | 0.1840 | −6.9 | Borg et al. (2016) | | | | |
| NWA 1068 | −6.1 | 0.1849 | −6.3 | Borg et al. (2016) | | | | |
| NWA 4468 | −6.9 | 0.1834 | −7.2 | Borg et al. (2016) | | | | |
| | −6.7 | 0.1833 | −7.3 | Borg et al. (2016) | | | | |
| LAR 06319 | −7.1 | 0.1832 | −7.3 | Shafer et al. (2010) | −18.6 | 0.0276 | −18.4 | Shafer et al. (2010) |
| RBT 04261/04262 | −6.4 | 0.1846 | −6.5 | Shih et al. (2009) | | | | |
| Intermediate shergottites | | | | | | | | |
| EET 79001 (A) | 17.6 | 0.2259 | 17.1 | Debaille et al. (2007) | 32.5 | 0.0444 | 32.8 | Debaille et al. (2008) |
| | 17.1 | 0.2248 | 16.5 | Borg et al. (2016) | 33.5 | 0.0447 | 33.8 | Blichert-Toft et al. (1999) |
| EET 79001 (B) | 16.8 | 0.2244 | 16.3 | Nyquist et al. (2001) | 32.3 | 0.0443 | 32.7 | Blichert-Toft et al. (1999) |
| | | | | | 32.5 | 0.0444 | 32.8 | Blichert-Toft et al. (1999) |
| | | | | | 28.6 | 0.0431 | 28.9 | Blichert-Toft et al. (1999) |
| | | | | | 36.3 | 0.0456 | 36.7 | Blichert-Toft et al. (1999) |
| NWA 480 | 12.7 | 0.2145 | 10.8 | Borg et al. (2016) | | | | |
| LEW 88516 | 9.9 | 0.2128 | 9.6 | Borg et al. (2002) | | | | |
| ALH 77005 | 13.6 | 0.2187 | 13.0 | Borg et al. (2002) | 31.3 | 0.0440 | 31.8 | Blichert-Toft et al. (1999) |
| | | | | | 31.8 | 0.0442 | 32.3 | Blichert-Toft et al. (1999) |
| Y 793605 | 10.9 | 0.2139 | 10.3 | Misawa et al. (2006) | | | | |
| Y 984028 | 12.6 | 0.2173 | 12.2 | Shih et al. (2011) | | | | |
| Y 000097 | 12.2 | 0.2172 | 12.1 | Misawa et al. (2008) | | | | |
| Depleted shergottites | | | | | | | | |
| Sayh al | 46.9 | 0.2625 | 38.3 | Borg et al. (2016) | | | | |
| Uhaymir | 46.4 | 0.2634 | 38.9 | Debaille et al. (2007) | 49.3 | 0.0502 | 51.3 | Debaille et al. (2008) |
| 005/008/094 | 50.2 | 0.2689 | 42.0 | Debaille et al. (2007) | 46.7 | 0.0494 | 48.9 | Debaille et al. (2008) |
| Dar al Gani 476 | 51.3 | 0.2689 | 42.0 | Debaille et al. (2007) | 51.9 | 0.0509 | 53.7 | Debaille et al. (2008) |
| | 50.2 | 0.2649 | 39.7 | Borg et al. (2016) | | | | |
| Dhofar 019 | 44.9 | 0.2631 | 38.8 | Borg et al. (2016) | | | | |
| QUE 94201 | 54.1 | 0.2814 | 49.1 | Borg et al. (1997) | 40.8 | 0.0479 | 44.1 | Blichert-Toft et al. (1999) |
| | | | | | 36.6 | 0.0466 | 40.0 | Blichert-Toft et al. (1999) |
| | | | | | 47.9 | 0.0502 | 50.9 | Blichert-Toft et al. (1999) |
| Tissint | 52.5 | 0.2768 | 46.7 | Grosshans (2016) | 56.4 | 0.0540 | 63.4 | Grosshans (2016) |
| | 52.1 | 0.2766 | 46.5 | Borg et al. (2016) | | | | |
| NWA 1195 | 48.9 | 0.2691 | 42.0 | Symes et al. (2008) | | | | |
| Y 980459 | 48.3 | 0.2622 | 38.2 | Shih et al. (2005) | | | | |
| NWA 7635 | 83.3 | 0.2944 | 58.7 | Lapen et al. (2017) | 171.0 | 0.0570 | 78.6 | Lapen et al. (2017) |
| NWA 8159 | 85.0 | 0.3154 | 70.9 | Herd et al. (2017) | | | | |
| | 65.6 | 0.2992 | 61.5 | Herd et al. (2017) | | | | |
| Orthopyroxenite | | | | | | | | |
| ALH 84001 | −6.9 | 0.1652 | 15.2 | Lapen et al. (2010) | 45.3 | 0.0204 | −35.6 | Lapen et al. (2010) |

Only studies where both the isotope ratio and the parent–daughter ratio have been published on the same aliquots have been included in this table of calculated source values. See Supplementary Table 3 for the measured ratios. In the majority of studies the Sm–Nd and Lu–Hf analyses were not performed on the same aliquots. All the literature data has been corrected to $^{146}Nd/^{144}Nd = 0.7219$.

[a] $\varepsilon^{143}Nd_{150Ma} = (\{[(^{143}Nd/^{144}Nd)_{meas.} - [(^{147}Sm/^{144}Nd)_{meas.} \times \{\exp(\lambda_{147} \times 1.5 \times 10^6\ yr) - 1\}]\}/\{(^{143}Nd/^{144}Nd)_{CHUR} - [(^{147}Sm/^{144}Nd)_{CHUR} \times \{\exp(\lambda_{147} \times 1.5 \times 10^6\ yr) - 1\}]\} - 1) \times 10^4$, where $\lambda_{147} = 6.539 \times 10^{-12}\ yr^{-1}$, $(^{143}Nd/^{144}Nd)_{CHUR} = 0.512630$ and $(^{147}Sm/^{144}Nd)_{CHUR} = 0.1960$ (Bouvier et al., 2008).

[b] See equation 3 in the supplementary information.

[c] As mentioned in the text the measured NWA 7034 ratios are taken as source composition, therefore unlike the other data in this table these values are not the result of the calculation in equation 3.

[d] See equation 4 in the supplementary information.

Please cite this article in press as: Armytage, R.M.G., et al. A complex history of silicate differentiation of Mars from Nd and Hf isotopes in crustal breccia NWA 7034. Earth Planet. Sci. Lett. (2018), https://doi.org/10.1016/j.epsl.2018.08.013

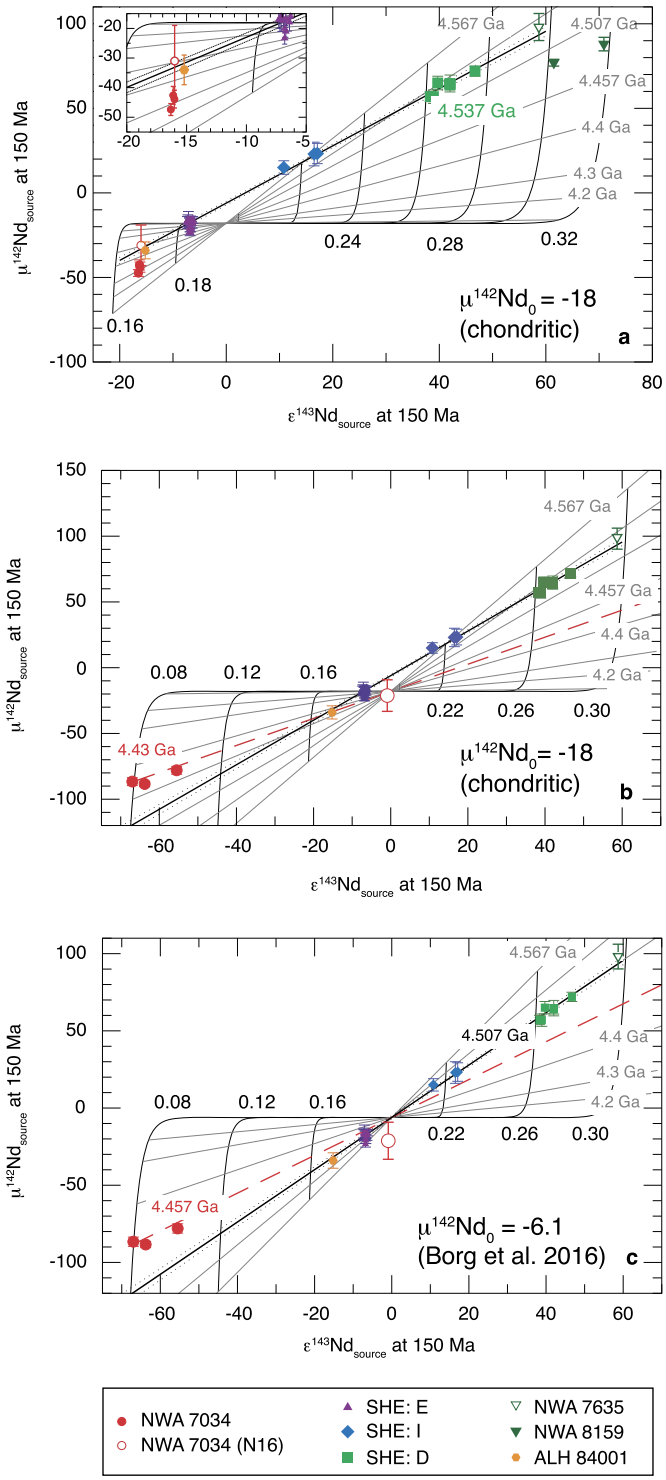


**Fig. 4.** Two-stage coupled $\mu^{142}$Nd–$\varepsilon^{143}$Nd evolution models projected to 150 Ma. The curved black lines are lines of equal $^{147}$Sm/$^{144}$Nd, plotted in increments of 0.02 (a) and 0.04 (b,c). The straight gray lines represent isochrons from 4.567 Ga to the present day (horizontal). The source compositions have been calculated and plotted for all the literature shergottite data (see Table 3 for references). Error bars in the *y*-direction represent measurement errors on $^{142}$Nd/$^{144}$Nd. The solid black line is the SSRL (shergottite source regression line), and the 95% confidence interval on the regression is also plotted. In (a) the initial $\mu^{142}$Nd is taken to be −18, and NWA 7034 is not corrected for $^{146}$Sm decay. In (b) NWA 7034 is corrected for $^{146}$Sm decay. In (c) NWA 7034 is corrected for $^{146}$Sm decay, and the initial $\mu^{142}$Nd of Mars is taken to be −6.1. In (b) and (c) NWA 8519 has been omitted for clarity, as it would plot in the same position as in (a).

In the first scenario the initial Nd isotopic composition of bulk Mars is assumed to be that of ordinary chondrites (Debaille et al., 2007), and the shergottite lavas mixed with the crust close to their eruption age. The three fragments of NWA 7034 do not fall on the shergottite source regression line (SSRL) but instead below it with lower $\mu^{142}$Nd values (Fig. 4a). In this scenario, the SSRL does not pass through the "origin" of the diagram where all the isochrons intersect. Hence the SSRL can only be interpreted as a mixing line, and no age constraint for global silicate differentiation in Mars can be extracted. In the second scenario bulk Mars is still assumed to be chondritic, however NWA 7034 is no longer taken to be a juvenile crust, and the mixing is between a "source" for the martian crust and shergottite sources, with NWA 7034 corrected for radiogenic ingrowth from $^{146}$Sm decay to its initial $\mu^{142}$Nd at its "age" at 4.4 Ga. In Fig. 4b the shergottite and NWA 7034 sources are all compared at 150 Ma; however, in this scenario mixing could have occurred at any time from 4.4 Ga to just prior to the crystallization of the shergottite magmas. With the correction for radiogenic ingrowth of $^{146}$Sm for NWA 7034, the age for silicate differentiation of the crustal reservoir is 4.43 Ga, consistent with the previously reported 4.428 Ga zircon ages (Humayun et al., 2013) and the $^{147}$Sm–$^{143}$Nd isochron age of 4.42 Ga ± 0.07 (Nyquist et al., 2016). However, age correction does not move NWA 7034 onto the SSRL mixing line, but instead in the opposite direction for $\mu^{142}$Nd (Fig. 4b). The younger age recorded by NWA 7034, relative to the source model age of 4.537 Ga for the depleted shergottites, could be consistent with a later martian crustal differentiation event possibly triggered by mantle overturn processes ~100 Ma after SSF (Debaille et al., 2009; Elkins-Tanton, 2005). In the third scenario, the constraint that Mars has a chondritic initial isotopic composition is relaxed, as recent high precision measurements of Nd isotopes (Bouvier and Boyet, 2016; Burkhardt et al., 2016) have exposed anomalies in solar system materials due to nucleosynthetic variations. As such the origin of the diagram can be moved (Fig. 4c) so that the SSRL intersects the origin, and is now an isochron with a 4.507 Ga closure age and a bulk Mars with a present-day $\mu^{142}$Nd value of −6.1 (Borg et al., 2016). This ~60 Ma isochron closure age after solar system formation of the $^{146,147}$Sm–$^{142,143}$Nd chronometers in the shergottite sources could potentially be the mean age of MMO crystallization. In this scenario, even with a different initial $\mu^{142}$Nd for bulk Mars, the martian crust as represented by NWA 7034 does not plot on the SSRL (Fig. 4c). Its model silicate differentiation age of 4.457 Ga is still younger than the SSRL isochron at 4.507 Gyr and makes the age gap between the crustal differentiation and the zircon crystallization age of 4.428 Ga greater, though conceivably within uncertainty given the brecciated nature of NWA 7034. As with the $^{147}$Sm/$^{144}$Nd versus $^{177}$Lu/$^{177}$Hf systematics, in all three scenarios the source composition of ALH 84001 plots on the SSRL, providing further evidence for a genetic link between the ALH 84001 source and the shergottite sources unlike NWA 7034. However, ALH 84001 itself cannot represent the enriched reservoir as in $\varepsilon^{143}$Nd (and $\varepsilon^{176}$Hf) versus La/Yb (Fig. 2a&b) it falls off the shergottite array. The fact that NWA 7034 falls so far off the SSRL weakens the argument for using any such "planetary isochron" for Mars to infer its bulk initial $\mu^{142}$Nd. The coupled $\varepsilon^{182}$W–$\mu^{142}$Nd systematics of martian meteorites (Kruijer et al., 2017) has highlighted how unlikely it is that the SSRL is in fact an isochron and the findings presented here are consistent with this conclusion. In either case, the coupled $^{146,147}$Sm–$^{142,143}$Nd models in these three scenarios confirm what is observed in the $^{147}$Sm/$^{144}$Nd versus $^{177}$Lu/$^{177}$Hf systematics, that the martian crust as represented by NWA 7034 cannot contribute in a significant way to the formation of the shergottite sources.

Arguably, the "rock" age for NWA 7034, as opposed to crystallization ages of minerals in clasts, is the most poorly constrained

parameter used in the models. The "rock" age represents an average Sm–Nd closure age rather than a crystallization age or lithification age (McCubbin et al., 2016). An older "rock" age, would push back the model age for crustal differentiation (Supplementary Fig. 2), having a greater effect than proposed range of initial Nd isotopic compositions of Mars. For the age of crustal differentiation (the isochrons in Fig. 4) to be consistent with an early differentiation of Mars (20–40 Ma after SSF), as proposed by the coupled $\varepsilon^{182}$W–$\mu^{142}$Nd systematics on bulk martian meteorites (Kruijer et al., 2017), the "rock" age would have to be closer to 4.51 Ga. However, no matter what the "rock" age, the decay corrected $\varepsilon^{143}$Nd, and $\mu^{142}$Nd data for NWA 7034, do not intersect with the SSRL, indicating the robustness of the conclusion that the martian crust represented by NWA 7034 did not contribute to shergottite compositional variability.

### 4.2. Formation of NWA 7034 crust

Having ruled out the crust represented by NWA 7034 as being the enriched end-member for the shergottites, we now focus on the formation of the crustal reservoir represented by NWA 7034. The rare earth element profile of NWA 7034 cannot be readily explained by melting of a depleted martian mantle (DMM) source (i.e. the cumulates of a MMO). One possible scenario is, like the enriched shergottite source, the crustal reservoir has itself been contaminated by late stage MMO liquids prior to ~4.4 Ga ("age" of NWA 7034) during a mantle overturn when the deep cumulate melted by adiabatic decompression (Debaille et al., 2009). However, a calculation of the initial (= source) $^{176}$Lu/$^{177}$Hf and $^{147}$Sm/$^{144}$Nd for NWA 7034 gives $^{176}$Lu/$^{177}$Hf = 0.02–0.04 and $^{147}$Sm/$^{144}$Nd ~0.05. These source $^{176}$Lu/$^{177}$Hf and $^{147}$Sm/$^{144}$Nd values are significantly higher and lower, respectively, than those expected for late stage liquids representing the end members in the mixing lines with martian mantle cumulates generated by a solidifying MMO during a mantle overturn (Fig. 3). In addition, the calculated $^{147}$Sm/$^{144}$Nd of 0.05 for NWA 7034 is unrealistically low, such that any modeling of the associated $\varepsilon^{143}$Nd–$\mu^{142}$Nd systematics gives aberrant values such as negative mixing fractions when previous modeling constraints on the evolution of the enriched reservoir (Debaille et al., 2007) are incorporated. The $\Delta^{17}$O of NWA 7034 is anomalous compared to other martian meteorites, and it has been proposed this could reflect either isolated lithospheric reservoirs or surficial atmospheric exchange (Agee et al., 2013). Considering it would be difficult for Mars to avoid at least a shallow magma ocean (Elkins-Tanton, 2005) and considering the need for a MMO to explain the shergottite enriched end-member as developed here, we favor the second hypothesis.

The low initial $^{147}$Sm/$^{144}$Nd ratio of NWA 7034 is likely the result of a multi-stage formation of this early crustal reservoir, ruling out that the bulk signatures reflect juvenile crust, and limiting the constraints possible on the precise timing of events in the martian mantle. The $^{146,147}$Sm–$^{142,143}$Nd and $^{176}$Lu–$^{176}$Hf systematics from this study along with the U–Pb dating of zircons and plagioclases (Bellucci et al., 2015; Humayun et al., 2013), and the diversity of igneous lithologies (Santos et al., 2015), point to NWA 7034 sampling a crust that underwent multiple stages of melting, and re-melting coupled with ongoing mantle differentiation during the first ~150 Myr of Mars' history. The recent $^{176}$Lu–$^{176}$Hf U-Pb zircon study of Bouvier et al. (2018) also requires that Mars' primordial crust was re-worked within the first 100 Myr of its history (note added in proof).

The precise physical model of how this crust is isolated from the shergottites sources, to the extent that its isotopic signature is not reflected in the shergottites, is unclear. However, this study of NWA 7034 further highlights the chemical and isotopic heterogeneity of the martian mantle.

## 5. Conclusions

The coupled $^{146,147}$Sm–$^{142,143}$Nd and $^{176}$Lu–$^{176}$Hf systematics for NWA 7034 are not consistent with a model where the crust it represents contributed to the source(s) of the shergottites. This is true whether the mixing happened within the first few hundred million years of martian history or just prior to the crystallization of the shergottites lavas, and whether bulk Mars is isotopically chondritic or not. Because the shergottites span a large range of ejection ages from ~1 Myr to ~18 Myr (Lapen et al., 2017), and their distribution on the martian surface could thus be more widespread than often considered, their source mixing line in $\varepsilon^{143}$Nd–$\mu^{142}$Nd space has to represent a global event affecting Mars. This conclusion holds independently of the mismatch in elemental composition between shergottites and spacecraft data of the surface, because it concerns sources deep in the mantle. As such, the high precision Hf and Nd isotopic compositions of the shergottites are best represented at present by the crystallization of a magma ocean progressively enriched in incompatible trace elements. By contrast, the coupled $^{146,147}$Sm–$^{142,143}$Nd and $^{176}$Lu–$^{176}$Hf systematics in NWA 7034 cannot easily explain the formation of a juvenile NWA 7034 like crust within the context of mixing of enriched and depleted reservoirs from a martian magma ocean. Instead, NWA 7034 compositional characteristics are consistent with this rock representing reworked crust with a multistage formation history. This further highlights the need for additional ancient crustal samples from Mars, either as meteorites or returned igneous samples.

## Acknowledgements

RMGA and VD would like to thank Wendy Debouge and Sabrina Cauchies for assistance in the lab, Jeroen De Jong for keeping the instruments in top condition, and Ashlea Wainwright for providing the terrestrial Sm cuts. RMGA and VD thank the ERC StG Grant 336718 "ISoSyC" for funding this study. VD also acknowledges support from FRS-FNRS for present funding and ADB acknowledges support from NASA grant NNX16AI28G.

## Appendix A. Supplementary material

Supplementary material related to this article can be found online at https://doi.org/10.1016/j.epsl.2018.08.013.

## References

Agee, C.B., Wilson, N.V., McCubbin, F.M., Ziegler, K., Polyak, V.J., Sharp, Z.D., Asmerom, Y., Nunn, M.H., Shaheen, R., Thiemens, M.H., Steele, A., Fogel, M.L., Bowden, R., Glamoclija, M., Zhang, Z., Elardo, S.M., 2013. Unique meteorite from Early Amazonian Mars: water-rich basaltic breccia Northwest Africa 7034. Science 339, 780–785. https://doi.org/10.1126/science.1228858.

Anders, E., Grevesse, N., 1989. Abundances of the elements: meteoritic and solar. Geochim. Cosmochim. Acta 53, 197–214. https://doi.org/10.1016/0016-7037(89)90286-x.

Bellucci, J.J., Nemchin, A.A., Whitehouse, M.J., Humayun, M., Hewins, R., Zanda, B., 2015. Pb-isotopic evidence for an early, enriched crust on Mars. Earth Planet. Sci. Lett. 410, 34–41. https://doi.org/10.1016/j.epsl.2014.11.018.

Blichert-Toft, J., Chauvel, C., Albarède, F., 1997. Separation of Hf and Lu for high-precision isotope analysis of rock samples by magnetic sector-multiple collector ICP-MS. Contrib. Mineral. Petrol. 127, 248–260. https://doi.org/10.1007/s004100050278.

Blichert-Toft, J., Gleason, J.D., Télouk, P., 1999. The Lu–Hf isotope geochemistry of shergottites and the evolution of the Martian mantle–crust system. Earth Planet. Sci. Lett. 173, 25–39. https://doi.org/10.1016/s0012-821x(99)00222-8.

Borg, L.E., Draper, D.S., 2003. A petrogenetic model for the origin and compositional variation of the martian basaltic meteorites. Meteorit. Planet. Sci. 38, 1713–1731. https://doi.org/10.1111/j.1945-5100.2003.tb00011.x.

Borg, L.E., Nyquist, L.E., Taylor, L.A., Wiesmann, H., Shih, C.-Y., 1997. Constraints on Martian differentiation processes from Rb–Sr and Sm–Nd isotopic analyses of the basaltic shergottite QUE 94201. Geochim. Cosmochim. Acta 61, 4915–4931. https://doi.org/10.1016/s0016-7037(97)00276-7.

Borg, L.E., Nyquist, L.E., Wiesmann, H., Reese, Y., 2002. Constraints on the petrogenesis of Martian meteorites from the Rb–Sr and Sm–Nd isotopic systematics of the lherzolitic shergottites ALH77005 and LEW88516. Geochim. Cosmochim. Acta 66, 2037–2053.

Borg, L.E., Nyquist, L.E., Wiesmann, H., Shih, C.-Y., Reese, Y., 2003. The age of Dar al Gani 476 and the differentiation history of the martian meteorites inferred from their radiogenic isotopic systematics. Geochim. Cosmochim. Acta 67, 3519–3536.

Borg, L.E., Brennecka, G.A., Symes, S.J.K., 2016. Accretion timescale and impact history of Mars deduced from the isotopic systematics of martian meteorites. Geochim. Cosmochim. Acta 175, 150–167. https://doi.org/10.1016/j.gca.2015.12.002.

Bouvier, A., Boyet, M., 2016. Primitive Solar System materials and Earth share a common initial $^{142}$Nd abundance. Nature 537, 399–402. https://doi.org/10.1038/nature19351.

Bouvier, A., Vervoort, J.D., Patchett, P.J., 2008. The Lu–Hf and Sm–Nd isotopic composition of CHUR: constraints from unequilibrated chondrites and implications for the bulk composition of terrestrial planets. Earth Planet. Sci. Lett. 273, 48–57.

Bouvier, L.C., Costa, M.M., Connelly, J.N., Jensen, N.K., Wielandt, D., Storey, M., et al., 2018. Evidence for extremely rapid magma ocean crystallization and crust formation on Mars. Nature 558 (7711), 586.

Brandon, A.D., Puchtel, I.S., Walker, R.J., Day, J.M.D., Irving, A.J., Taylor, L.A., 2012. Evolution of the martian mantle inferred from the $^{187}$Re–$^{187}$Os isotope and highly siderophile element abundance systematics of shergottite meteorites. Geochim. Cosmochim. Acta 76, 206–235. https://doi.org/10.1016/j.gca.2011.09.047.

Brennecka, G.A., Borg, L.E., Wadhwa, M., 2014. Insights into the Martian mantle: the age and isotopics of the meteorite fall Tissint. Meteorit. Planet. Sci. 49, 412–418.

Burkhardt, C., Borg, L.E., Brennecka, G.A., Shollenberger, Q.R., Dauphas, N., Kleine, T., 2016. A nucleosynthetic origin for the Earth's anomalous $^{142}$Nd composition. Nature 537, 394–398. https://doi.org/10.1038/nature18956.

Caro, G., Bourdon, B., Birck, J.L., Moorbath, S., 2006. High-precision $^{142}$Nd/$^{144}$Nd measurements in terrestrial rocks: constraints on the early differentiation of the Earth's mantle. Geochim. Cosmochim. Acta 70, 164–191. https://doi.org/10.1016/j.gca.2005.08.015.

Caro, G., Bourdon, B., Halliday, A.N., Quitte, G., 2008. Super-chondritic Sm/Nd ratios in Mars, the Earth and the Moon. Nature 452, 336–339. https://doi.org/10.1038/nature06760.

Cartwright, J.A., Ott, U., Herrmann, S., Agee, C.B., 2014. Modern atmospheric signatures in 4.4 Ga Martian meteorite NWA 7034. Earth Planet. Sci. Lett. 400, 77–87. https://doi.org/10.1016/j.epsl.2014.05.008.

Debaille, V., Brandon, A.D., Yin, Q.Z., Jacobsen, B., 2007. Coupled $^{142}$Nd–$^{143}$Nd evidence for a protracted magma ocean in Mars. Nature 450, 525–528. https://doi.org/10.1038/nature06317.

Debaille, V., Yin, Q.Z., Brandon, A.D., Jacobsen, B., 2008. Martian mantle mineralogy investigated by the $^{176}$Lu–$^{176}$Hf and $^{147}$Sm–$^{143}$Nd systematics of shergottites. Earth Planet. Sci. Lett. 269, 186–199.

Debaille, V., Brandon, A.D., O'Neill, C., Yin, Q.Z., Jacobsen, B., 2009. Early martian mantle overturn inferred from isotopic composition of nakhlite meteorites. Nat. Geosci. 2, 548–552.

Elkins-Tanton, L.T., 2005. Possible formation of ancient crust on Mars through magma ocean processes. J. Geophys. Res. 110, E12S01-11. https://doi.org/10.1029/2005JE002480.

Ferdous, J., Brandon, A.D., Peslier, A.H., Pirotte, Z., 2017. Evaluating crustal contributions to enriched shergottites from the petrology, trace elements, and Rb–Sr and Sm–Nd isotope systematics of Northwest Africa 856. Geochim. Cosmochim. Acta 211, 280–306.

Goderis, S., Brandon, A.D., Mayer, B., Humayun, M., 2016. Ancient impactor components preserved and reworked in martian regolith breccia Northwest Africa 7034. Geochim. Cosmochim. Acta 191, 203–215. https://doi.org/10.1016/j.gca.2016.07.024.

Grosshans, T., 2016. Lu–Hf and Sm–Nd Ages and Source Compositions for Depleted Shergottite Tissint. Thesis. https://uh-ir.tdl.org/uh-ir/bitstream/handle/10657/1215/GROSSHANS-THESIS-2013.pdf.

Herd, C.D.K., Borg, L.E., Jones, J.H., Papike, J.J., 2002. Oxygen fugacity and geochemical variations in the martian basalts: implications for martian basalt petrogenesis and the oxidation state of the upper mantle of Mars. Geochim. Cosmochim. Acta 66, 2025–2036.

Herd, C.D.K., Walton, E.L., Agee, C.B., Muttik, N., Ziegler, K., Shearer, C.K., Bell, A.S., Santos, A.R., Burger, P.V., Simon, J.I., Tappa, M.J., Mccubbin, F.M., Gattacceca, J., Lagroix, F., Sanborn, M.E., Yin, Q.-Z., Cassata, W.S., Borg, L.E., Lindvall, R.E., Kruijer, T.S., Brennecka, G.A., Kleine, T., Nishiizumi, K., Caffee, M.W., 2017. The Northwest Africa 8159 martian meteorite: expanding the martian sample suite to the early Amazonian. Geochim. Cosmochim. Acta 218, 1–26. https://doi.org/10.1016/j.gca.2017.08.037.

Hewins, R.H., Zanda, B., Humayun, M., Nemchin, A., Lorand, J.-P., Pont, S., Deldicque, D., Bellucci, J.J., Beck, P., Leroux, H., Marinova, M., Remusat, L., Gopel, C., Lewin, E., Grange, M., Kennedy, A., Whitehouse, M.J., 2016. Regolith breccia Northwest Africa 7533: mineralogy and petrology with implications for early Mars. Meteorit. Planet. Sci. 52, 89–124. https://doi.org/10.1111/maps.12740.

Humayun, M., Nemchin, A., Zanda, B., Hewins, R.H., Grange, M., Kennedy, A., Lorand, J.-P., Göpel, C., Fieni, C., Pont, S., Deldicque, D., 2013. Origin and age of the earliest Martian crust from meteorite NWA7533. Nature 503, 513–516. https://doi.org/10.1038/nature12764.

Kruijer, T.S., Kleine, T., Borg, L.E., Brennecka, G.A., Irving, A.J., Bischoff, A., Agee, C.B., 2017. The early differentiation of Mars inferred from Hf–W chronometry. Earth Planet. Sci. Lett. 474, 345–354. https://doi.org/10.1016/j.epsl.2017.06.047.

Langmuir, C.H., Vocke, R.D., Hanson, G.N., Hart, S.R., 1978. A general mixing equation with applications to Icelandic basalts. Earth Planet. Sci. Lett. 37, 380–392.

Lapen, T.J., Righter, M., Brandon, A.D., Debaille, V., Beard, B.L., Shafer, J.T., Peslier, A.H., 2010. A Younger age for ALH84001 and its geochemical link to shergottite sources in Mars. Science 328, 347–351. https://doi.org/10.1126/science.1185395.

Lapen, T.J., Righter, M., Andreasen, R., Irving, A.J., Satkoski, A.M., Beard, B.L., Nishiizumi, K., Jull, A.J.T., Caffee, M.W., 2017. Two billion years of magmatism recorded from a single Mars meteorite ejection site. Sci. Adv. 3, e1600922. https://doi.org/10.1126/sciadv.1600922.

Li, C.-F., Wang, X.-C., Li, Y.-L., Chu, Z.-Y., Guo, J.-H., Li, X.-H., 2015. Ce–Nd separation by solid-phase micro-extraction and its application to high-precision $^{142}$Nd/$^{144}$Nd measurements using TIMS in geological materials. J. Anal. At. Spectrom. 4, 1–8. https://doi.org/10.1039/C4JA00328D.

McCubbin, F.M., Boyce, J.W., Novák-Szabó, T., Santos, A.R., Tartèse, R., Muttik, N., Domokos, G., Vazquez, J., Keller, L.P., Moser, D.E., Jerolmack, D.J., Shearer, C.K., Steele, A., Elardo, S.M., Rahman, Z., Anand, M., Delhaye, T., Agee, C.B., 2016. Geologic history of Martian regolith breccia Northwest Africa 7034: evidence for hydrothermal activity and lithologic diversity in the Martian crust. J. Geophys. Res., Planets 121, 2120–2149. https://doi.org/10.1002/2016JE005143.

McDonough, W., Sun, S., 1995. The composition of the Earth. Chem. Geol. 120, 223–253.

McSween, H.Y., Taylor, G.J., Wyatt, M.B., 2009. Elemental composition of the martian crust. Science 324, 736–739. https://doi.org/10.1126/science.1165871.

Meissner, F., Schmidt-Ott, W.D., Ziegeler, L., 1987. Half-life and $\alpha$-ray energy of $^{146}$Sm. Z. Phys. A 327, 171–174. https://doi.org/10.1007/BF01292406.

Misawa, K., Yamada, K., Nakamura, N., Morikawa, N., Yamashita, K., Premo, W.R., 2006. Sm–Nd isotopic systematics of lherzolitic shergottite Yamato-793605. Antarct. Meteor. Res., 45–57.

Misawa, K., Park, J., Shih, C.Y., Reese, Y., Bogard, D.D., Nyquist, L.E., 2008. Rb–Sr, Sm–Nd, and Ar–Ar isotopic systematics of lherzolitic shergottite Yamato 000097. Polar Sci. 2, 163–174.

Nyquist, L.E., Wiesmann, H., Bansal, B., Shih, C.Y., Keith, J.E., Harper, C.L., 1995. $^{146}$Sm–$^{142}$Nd formation interval for the lunar mantle. Geochim. Cosmochim. Acta 59, 2817–2837. https://doi.org/10.1016/0016-7037(95)00175-y.

Nyquist, L.E., Bogard, D.D., Shih, C.Y., Greshake, A., 2001. Ages and geologic histories of Martian meteorites. Space Sci. Rev. 12, 105–164.

Nyquist, L.E., Shih, C.-Y., McCubbin, F.M., Santos, A.R., Shearer, C.K., Peng, Z.X., Burger, P.V., Agee, C.B., 2016. Rb–Sr and Sm–Nd isotopic and REE studies of igneous components in the bulk matrix domain of Martian breccia Northwest Africa 7034. Meteorit. Planet. Sci. 51, 483–498. https://doi.org/10.1111/maps.12606.

Rankenburg, K., Brandon, A.D., Neal, C.R., 2006. Neodymium isotope evidence for a chondritic composition of the Moon. Science 312, 1369–1372. https://doi.org/10.1126/science.1126114.

Santos, A.R., Agee, C.B., McCubbin, F.M., Shearer, C.K., Burger, P.V., Tartèse, R., Anand, M., 2015. Petrology of igneous clasts in Northwest Africa 7034: implications for the petrologic diversity of the martian crust. Geochim. Cosmochim. Acta 157, 56–85. https://doi.org/10.1016/j.gca.2015.02.023.

Shafer, J.T., Brandon, A.D., Lapen, T.J., Righter, M., Peslier, A.H., Beard, B.L., 2010. Trace element systematics and $^{147}$Sm–$^{143}$Nd and $^{176}$Lu–$^{176}$Hf ages of Larkman Nunatak 06319: closed-system fractional crystallization of an enriched shergottite magma. Geochim. Cosmochim. Acta 74, 7307–7328. https://doi.org/10.1016/j.gca.2010.09.009.

Shih, C.Y., Nyquist, L.E., Wiesmann, H., Reese, Y., Misawa, K., 2005. Rb–Sr and Sm–Nd dating of olivine-phyric shergottite Yamato 980459: petrogenesis of depleted shergottites. Antarct. Meteor. Res. 18, 46.

Shih, C.Y., Nyquist, L.E., Reese, Y., 2009. Rb–Sr and Sm–Nd studies of olivine-phyric shergottites RBT 04262 and LAR 06319: isotopic evidence for relationship to enriched basaltic shergottites. Lunar Planet. Sci. Conf. 40, 1360.

Shih, C.Y., Nyquist, L.E., Reese, Y., Misawa, K., 2011. Sm–Nd and Rb–Sr studies of lherzolitic shergottite Yamato 984028. Polar Sci. 4, 515–529.

Sprung, P., Kleine, T., Scherer, E.E., 2013. Isotopic evidence for chondritic Lu/Hf and Sm/Nd of the Moon. Earth Planet. Sci. Lett. 380, 77–87. https://doi.org/10.1016/j.epsl.2013.08.018.

Symes, S.J.K., Borg, L.E., Shearer, C.K., Irving, A.J., 2008. The age of the martian meteorite Northwest Africa 1195 and the differentiation history of the shergottites. Geochim. Cosmochim. Acta 72, 1696–1710.

Tanaka, T., Togashi, S., Kamioka, H., Amakawa, H., Kagami, H., Hamamoto, T., Yuhara, M., Orihashi, Y., Yoneda, S., Shimizu, H., Kunimaru, T., Takahashi, K., Yanagi, T., Nakano, T., Fujimaki, H., Shinjo, R., Asahara, Y., Tanimizu, M., Dragusanu, C., 2000. JNdi-1: a neodymium isotopic reference in consistency with LaJolla neodymium. Chem. Geol. 168, 279–281. https://doi.org/10.1016/S0009-2541(00)00198-4.

Weis, D., Kieffer, B., Maerschalk, C., Barling, J., de Jong, J., Williams, G.A., Hanano, D., Pretorius, W., Mattielli, N., Scoates, J.S., Goolaerts, A., Friedman, R.M., Mahoney, J.B., 2006. High-precision isotopic characterization of USGS reference materials

Please cite this article in press as: Armytage, R.M.G., et al. A complex history of silicate differentiation of Mars from Nd and Hf isotopes in crustal breccia NWA 7034. Earth Planet. Sci. Lett. (2018), https://doi.org/10.1016/j.epsl.2018.08.013

by TIMS and MC-ICP-MS. Geochem. Geophys. Geosyst. 7, Q08006. https://doi.org/10.1029/2006GC001283.

Weis, D., Kieffer, B., Hanano, D., Silva, I.N., Barling, J., Pretorius, W., Maerschalk, C., Mattielli, N., 2007. Hf isotope compositions of US Geological Survey reference materials. Geochem. Geophys. Geosyst. 8, Q06006. https://doi.org/10.1029/2006GC001473.

Wilson, S.A., 1997. Data Compilation for USGS Reference Material BHVO-2, Hawaiian Basalt. US Geological Survey Open-file Report.

Please cite this article in press as: Armytage, R.M.G., et al. A complex history of silicate differentiation of Mars from Nd and Hf isotopes in crustal breccia NWA 7034. Earth Planet. Sci. Lett. (2018), https://doi.org/10.1016/j.epsl.2018.08.013